SCIENCE CHINA
Life Sciences

• COVER ARTICLE •

November 2017 Vol.60 No.11: 1157–1167
doi: 10.1007/s11427-017-9055-x

Morphological evaluation of retinal ganglion cells expressing the L132C/T159C ChR2 mutant transgene in young adult cynomolgus monkeys

Wenyao Wang[1], Yan Nan[1], Zhuo-Hua Pan[2*] & Mingliang Pu[1*]

[1]*Department of Embryology/Anatomy, School of Basic Medical Sciences, Peking University, Beijing 100191, China;*
[2]*Department of Ophthalmology and Anatomy/Cell Biology, Wayne State University School of Medicine, Detroit Michigan 48201, USA*

Received March 17, 2017; accepted April 3, 2017; published online May 25, 2017

To characterize recombinant AAV2 (rAAV2)-mediated expression of L132C/T159C ChR2 mutant in retinal ganglion cells (RGCs) of young adult cynomolgus monkeys, rAAV2 vectors carrying a fusion construct of the ChR2 mutant and GFP (ChR2-GFP) were delivered to the vitreous chamber by intravitreal injection. Expression patterns of the ChR2 mutant in RGCs were examined by immunohistochemical methods three months after injection. The RNA-binding protein with multiple splicing (RBPMS) was used as an RGC specific marker to differentiate RGCs from other retinal neurons and non-neuronal cells. The numbers of $RBPMS^+$ and GFP^+ double-labeled RGCs in the central foveal varied with the eccentricity. The expression peaked within 100 μm from the edge of the foveola and drastically decreased to a single superficial RGC layer approximately 300 μm from the edge. On average, the ratio of the double-labeled RGCs versus $RBPMS^+$ RGCs approached 0.32±0.15 (n=14 fields) at the central foveal region (0.1 to 0.53 mm). We observed that the ratio reached 0.78±0.16 (n=21 fields) at peripheral retinal locations (eccentricity >7 mm). This investigation demonstrates that RBPMS could serve as a valuable RGC specific marker for future investigations in this field.

ChR2 mutant transgene, retinal ganglion cells, cynomolgus monkey

Citation: Wang, W., Nan, Y., Pan, Z.H., and Pu, M. (2017). Morphological evaluation of retinal ganglion cells expressing the L132C/T159C ChR2 mutant transgene in young adult cynomolgus monkeys. Sci China Life Sci 60, 1157–1167. doi: 10.1007/s11427-017-9055-x

INTRODUCTION

Since the discovery of native ChR1 and ChR2 (Nagel et al., 2002; Nagel et al., 2003), there have been reports of many ChR2 mutants and ChR variants with altered light response properties, including increased photocurrents (Mattis et al., 2011; Nagel et al., 2005; Zhang et al., 2008; Wang et al., 2009; Lin et al., 2009; Berndt et al., 2011; Kleinlogel et al., 2011; Yizhar et al., 2011). However, a major hurdle in the use of native ChR2 as a light sensor for vision restoration is the low light sensitivity of ChR2-expressing RGCs, approximately four log units lower than that of cones (Bi et al., 2006). Recently, the light-evoked response properties of two of the most light-responsive mutants, L132C/T159C and L132C/T159S, were characterized in adult C57BL/6J mice (Pan et al., 2014). It was observed that the required light intensities for generating the threshold spiking activity in retinal ganglion cells were 1.5 and nearly two log units lower than wild-type ChR2, respectively. Temporally, ChR2-mediated spiking activities of these RGCs could follow flicker

*Corresponding authors (Zhuo-Hua Pan, email: zhpan@med.wayne.edu; Mingliang Pu, email: mpu@bjmu.edu.cn)

frequencies up to 20 and 10 Hz, respectively, at light intensities up to 1.5 log units above their threshold levels (Pan et al., 2014). However, the expression patterns of these transgenes have not been verified in retinas of large non-human primate species.

Despite proofs of concept in mice (Bi et al., 2006) and marmosets (a small non-human primate species, Ivanova et al., 2010), the expression efficacy of these new mutant transgenes has yet to be demonstrated in large nonhuman primate model. The cynomolgus monkey (*Macaca fascicularis*) is a large non-human primate species that is widely used for evaluating the safety and biodistribution of recombinant AAV2 (rAAV2) vectors for the treatment of various retinal diseases, such as age related macular degeneration (AMD) (Maclachlan et al., 2011), achromatopsia (Ye et al., 2016), Leber congenital amaurosis (Jacobson et al., 2006), retinal and choroidal neovascularization (Lai et al., 2005), retinal diseases originating in the RPE (Weber et al., 2003), and other ocular diseases (Buie et al., 2010). Thus, it is important to characterized the expression patterns of L132C/T159C and L132C/T159S ChR2 mutants in RGCs of young adult cynomolgus monkeys.

Previous studies revealed that, in addition to RGCs, many types of retinal neurons, such as horizontal cells, amacrine cells, and bipolar cells, as well as Müller cells (Bi et al., 2006; Ivanova and Pan, 2009; Ivanova et al., 2010) could be transfected. Similar observations were made by several investigators (Yin et al., 2011; Dalkara et al., 2009; Boyd et al., 2016). The area of transduction is restricted primarily to a "ring" of RGCs around the fovea (Ivanova et al., 2010; Yin et al., 2011; Dalkara et al., 2009; Boyd et al., 2016). However, to date, the exact number of ChR2-expressing RGCs remains to be determined. To quantify the number of ChR2-expressing RGCs, it is necessary to select a reliable RGC marker. It was reported recently that a member of the RNA recognition motif family of RNA-binding proteins, known as RNA-binding protein with multiple splicing (RBPMS), is expressed in all RGCs in the retinas of mouse, rat, guinea pig, rabbit, cat, and monkey (Piri et al., 2006; Kwong et al., 2010; Rodriguez et al., 2014; Wang et al., 2016; Liu et al., 2016). Together, these studies suggest that RBPMS can serve as a reliable RGC marker for future studies.

The purpose of the present study was to characterize the expression patterns of L132C/T159C ChR2 mutant in RGCs of young adult cynomolgus monkeys. By using GFP and RBPMS antibodies, we observed that the proportion of RGCs expressing the mutant transgene could reach 0.56 in the foveal region and increased to 0.70–0.90 at peripheral retinal locations. As with the wild-type ChR2, the present result suggests that this transgene can be expressed in many morphologically distinct RGCs in this species of primate. This study offers valuable information for a clinically relevant gene therapy for inner retinal degeneration.

RESULTS

Quantification of the ChR2 L132C/T159C transgene expressing ratio in RGCs in the foveola and other eccentric locations

Foveola region. It has been widely recognized that the transgene can be expressed not only in RGCs, but also in amacrine cells, bipolar cells, horizontal cells, and Müller cells (Bi et al., 2006; Ivanova and Pan, 2009; Ivanova et al., 2010). Thus, it has been difficult to objectively evaluate the transgene expression ratio in RGCs alone. To address this issue, we chose an RBPMS antibody as a selective RGC marker in this study. Thus, we used the RBPMS antibody to recognize RGCs and a GFP antibody to selectively label GFP-immunoreactive cells. By taking this approach, we could objectively analyze the transgene expression rate in RGCs. We selected various retinal locations from the fovea to the central retina and extended the evaluation to the peripheral retina. As shown in Figure 1, GFP antibody was applied to enhance the GFP signals (Figure 1A), the RBPMS antibody selectively detected RGCs (Figure 1B), and the merged image was shown in Figure 1C. The foveola was 490 μm in diameter. The size of the foveola was measured in four retinas and the average foveola size was (427±32) μm (n=4). The width of the foveal "ring" was approximately 224 μm. It appeared that GFP^+ cells unevenly distributed within the "ring". Next, five counting areas (0.0362 mm^2 $area^{-1}$) around the fovea were randomly selected (Figure 1D–H). As illustrated in Table 1 (Animal tissue ID: 13C02016R), the density of GFP and RBPMS double-labeled RGCs (GFP^+/$RBPMS^+$ RGCs) ranged from 5,442 to 7,624 per mm^2 and the average was 6,017±1,206. The density of $RBPMS^+$ RGCs varied from 10,718 to 13,619 per mm^2 and the average was 12,017±1,066. The ratio of GFP^+ to $RBPMS^+$ RGCs varied from 0.37 to 0.56 per site. On average the rate of encountering double-labeled RGCs in the foveal region was 0.5±0.08. Three more foveal retinas were selected and RGCs expressing the transgene in three counting areas per retina were analyzed. The results are summarized in Table 1. As listed in the Table, one of the animals showed relatively low densities of GFP-expressing RGCs (13C01086L: 1,519, 1,519, 1,575 cells mm^{-2}), while the other two exhibited relatively high expression densities (13C02016L: 2,569, 2,541, 2,265 cells mm^{-2}; 15C06024L: 2,762, 2,762, 2,376 cells mm^{-2}). To estimate the transgene expression ratio in the foveal region, we double stained a foveal retina and analyzed the GFP and RBPMS expression ratio in this retina (13C02016R). As shown in Figure 2A, the number of GFP^+ cells peaked at approximately 200 μm from the center, where approximately five layers of RGCs expressed GFP. Then, it quickly taped off, and occasionally RGCs in the superficial RGC layer also expressed GFP. Figure 2B shows that RBPMS-expressing RGCs, gradually

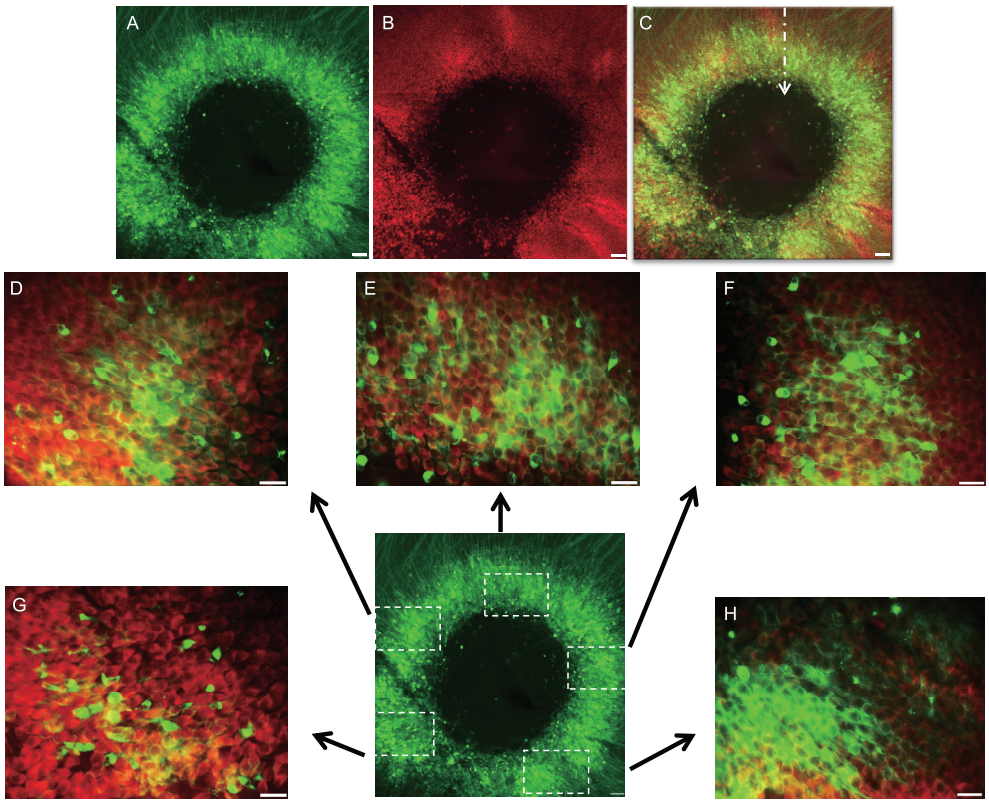

Figure 1 Foveal images of GFP$^+$ and RBPMS$^+$ double-labeled RGCs. A, GFP-immunostained neurons. B, RGC specific antibody (RBPMS) stained foveal RGCs. C, Merged image of panels A and B. The vertical arrowhead illustrates the image collection site for the foveal region. Scale bar: 50 μm. D–H, Quantitative analysis of GFP$^+$ RGCs. Five rectangular sampling areas around the fovea were randomly selected. Neurons expressing GFP and detectable using the RPBMS antibody are defined as double-labeled RGCs. Five merged images show GFP-expressing neurons (green) and in the background are neurons that are immunoreactive for the RBPMS antibody (red). As shown in the figures, the transgene expression around the fovea was not uniform. In comparison with other sampling areas, panel H had the most GFP$^+$ cells, followed by panels F, E, D, and G. Scale bar, 20 μm.

increased in the central fovea. A single layer of RBPMS immunoreactive-RGCs was clearly identifiable at the inner edge of the fovea (the first white arrowhead indicates the soma on the bottom of the confocal fluorescence image) and multiple layers of RGCs were detected beyond the edge. As revealed in the merged image (Figure 2C), the viral vector could only spread up to 200 μm laterally to reach multiple layers of RGCs. A further shift of 200 μm to the parafoveal direction resulted in few GFP$^+$ RGCs (a superficially located GFP$^+$ cell is indicated by a white arrowhead, at the uppermost edge of the micrograph).

Central retina. Next we counted double-stained central RGCs at different central retinal locations. Two eccentric sampling sites were randomly selected (numbers listed along the left column of Figure 3). GFP$^+$ RGCs are shown in the left column of the figure (Figure 3A and D); the RBPMS$^+$ RGCs are shown in the center column (Figure 3B and E), and the GFP$^+$/RBPMS$^+$ double-labeled RGCs are revealed in the right column (Figure 3C and F). As shown in Table 1, the densities of GFP$^+$/RBPMS+ double-labeled RGCs were 1,823 at 2.61 mm and 1,685 at 2.55 mm from the fovea. The densities of RGCs those expressed RBPMS at the same sample sites were 9,365 and 7,818, respectively. Finally, the ratios of GFP$^+$/RBPMS$^+$ vs. RBPMS$^+$ RGCs were 0.19 and 0.22, respectively. Occasionally, as shown in Figure 3A–F, some cells did not express GFP but were immunoreactive to RBPMS (white open arrowheads), while other cells did express GFP but did not express RBPMS (yellow open arrowheads).

Peripheral retina. RGCs situated at three peripheral locations, 7.62, 7.71, and 8.01 mm were analyzed (Figure 4A, D and G). RBPMS$^+$ RGCs are presented in the center column (Figure 4B, E and H); and GFP$^+$/RBPMS$^+$ double-labeled RGCs are exhibited in the right column (Figure 4C, F and I). The densities of double-labeled RGCs were 359 at 7.62 mm, 276 at 7.71 mm, and 470 at 8.01 mm from the fovea. The densities of RBPMS$^+$ cells at the same counting sites were 525, 359, and 773, respectively. Finally, the expressing ratios of the double-labeled vs. RBPMS$^+$ RGCs were 0.68, 0.77, and 0.61, respectively. As illustrated in Table 1, an additional total 34 counting sites from eccentricities 3 to 13.7 mm selected from four retinas were examined to quantify the expression ratio of double-labeled RGCs. First, 13C01086L shows that, between eccentricities 7 and 13, the averaged density of GFP$^+$/RBPMS$^+$ RGCs reached (5,011±1,598) mm^{-2}, that of RBPMS$^+$ RGCs was

Table 1 Double-labeled RGCs vs. RBPMS$^+$ RGCs ratio at different eccentric locations[a)]

Animal ID	Gender	Age at injection (Month)	Age at harvest (Month)	Expression duration (Month)	Tissue ID	Foveal site	ECCentricity (mm)	GFP$^+$ and RBPMS$^+$ density	RBPMS$^+$ density	Double label to RBPMS Ratio	Peripheral sites	Eccentricity (mm)	GFP$^+$ and RBPMS$^+$ density	RBPMS$^+$ density	Double label to RBPMS Ratio
13C01086	M	32	35	3	13C01086L	1	0.1	1,519	10,304	0.15	1	7.62	359	525	0.68
						2	0.14	1,519	7,983	0.19	2	7.71	276	359	0.77
						3	0.2	1,575	7,072	0.22	3	8.01	470	773	0.61
											4	11.24	166	221	0.75
											5	13.32	304	414	0.73
											6	13.7	304	497	0.61
13C08005	M	32	34	2	13C08005L*						1	2.55	1,685	7,818	0.22
											2	2.61	1,823	9,365	0.19
											3	3.47	773	4,448	0.17
											4	4.69	470	1,575	0.30
											5	7.50	193	470	0.41
											6	7.78	331	442	0.75
											7	10	193	193	1
											8	11.01	331	552	0.6
15C06024	M	16	18	2	15C06024L	1	0.2	2,762	9,807	0.28	1	7.56	359	387	0.93
						2	0.32	2,762	10,580	0.26	2	8.27	276	304	0.91
						3	0.32	2,376	10,497	0.23	3	8.77	331	331	1
					15C06024R						1	7.61	414	525	0.79
											2	8.37	193	193	1
											3	8.6	193	193	1
											4	8.84	442	497	0.89
											5	12.42	608	691	0.88
13C02016	M	31	34	3	13C02016L	1	0.22	2,569	10,166	0.25					
						2	0.28	2,541	10,580	0.24					
						3	0.36	2,265	11,077	0.2					
					13C02016R	1	0.29	5,442	10,718	0.51					
						2	0.34	4,392	11,796	0.37					
						3	0.36	7,624	13,619	0.56					
						4	0.37	6,105	12,320	0.5					
						5	0.53	6,519	11,630	0.56					

a) *, Only listed data collected eight counting sites, a complete set of data from a total of 25 counting sites from this retina was presented in results.

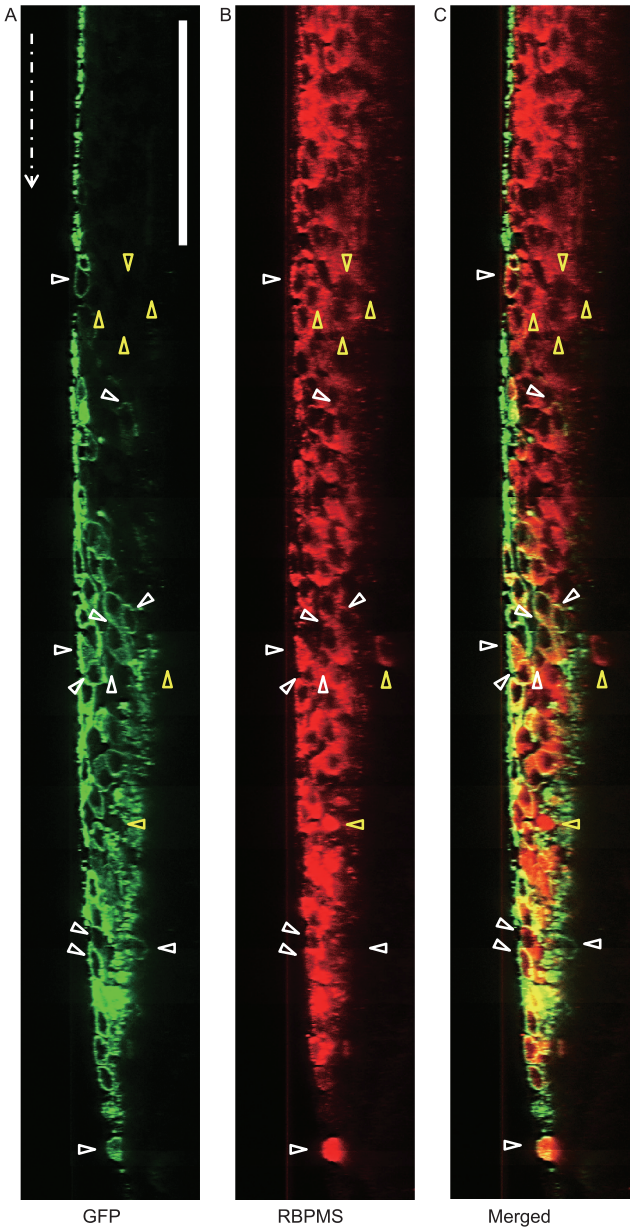

Figure 2 Confocal fluorescence image of a foveal retinal cross-section. A, Confocal micrograph (an averaged image of 16 0.605 μm optical sections) of GFP expression in the foveal retina that was double labeled for the RGC marker (RBPMS, red). The dashed vertical arrow points to the center of the foveola. B, RBPMS-expressing RGCs in the cross-section. The white arrowheads indicate RGCs immunoreactive to GFP and yellow arrowheads indicate RGCs those did not express GFP but did express RBPMS. As the thickness of the RGC layer increased, the number of RGCs expressing GFP quickly tapered off and only a few neurons in the deeper RGC layer expressed GFP. In addition, at more lateral locations, only RGCs those were located in the superficial RGC layer could express the transgene. The white arrowhead at the uppermost position in the image indicates a superficially located double-labeled cell. The number of RBPMS-labeled RGCs increased with eccentricity. As revealed by yellow arrowheads, more neurons expressed only RBPMS in the deeper RGC layer. C, Merged image of A and B.

(7,437±2,975) mm^{-2}, and the expression ratio of the two was 0.69±0.07. Retinas 15C06024R and 15C06024L were from the same animal. As shown in Table 1, data from eight counting sites between eccentricities of 7.56 and 12.42 mm were collected and analyzed. The average density of double-labeled RGCs was (352±139) mm^{-2}, that of $RBPMS^+$ RGCs was (390±173) mm^{-2}, and the expression ratio of the two was 0.92±0.07. The most peripheral retinal data was collected from 13C08005L. Twenty-five counting sites from eccentricities 3 to 13.7 mm were randomly collected. Since the expression ratio varied with the eccentricity, the data analysis was divided into three parts. Six counting sites were selected between eccentricities of 3 to 4.05 mm, for which the averaged density of double-labeled RGCs was (1,257±686) mm^{-2}, that of $RBPMS^+$ RGCs was (4,820±1,746) mm^{-2}, and the expression ratio of the two was 0.26±0.08. Between the eccentricities of 4.27 and 7.78 mm, the average density of double-labeled RGCs was (417±226) mm^{-2}, that of $RBPMS^+$ RGCs was (1,436±1,098) mm^{-2}, and the expression ratio of the two was 0.36±0.15. For eccentricities greater than 10 mm, five counting sites were selected. The averaged density of double-labeled RGCs was (398±198) mm^{-2}, that of $RBPMS^+$ RGCs was (563±255) mm^{-2} and the expression ratio of the two was 0.73±0.18. These data are summarized in Figure 5. It is evident that the ratio of encountering double-labeled RGCs increased with eccentricity, but few trangenic RGCs was identified between eccentricities of 0.5 and 2 mm. To objectively estimate the transgene expression ratio at remote peripheral retina (eccentricity >7 mm), we collected data from four retinas and analyzed the average transgene expression ratio, these results show that the averaged ratio was 0.78±0.16.

Morphology of the transgene expressing RGCs

Morphology of the transgene expressing RGCs was closely examined. As shown in Figure 6, the transgene expressing RGCs were encountered at different retinal locations and eccentricities. At 4.27 mm from the fovea (Panel A), one of the labeled cells showed midget cell morphology (soma: red arrowhead, axon: white open arrowhead). The color-coded depth indicator in the lower right corner illustrates the soma location in the RGC layer and the dendritic process ramification levels in the inner plexiform layer (IPL). The warm colors are closer to the reader, and cooler colors are farther away from the reader. As shown in panel A, both somas of RGCs showed similar color, approximately 45 μm, but their dendritic processes were green suggesting that they ramified in a deeper level than that containing the soma. At another eccentric location (8.18 mm, Panel B), three midget cells (red arrowheads) near the center of the field were surrounded by three cells that shared similar dendritic morphological properties (white arrowheads). At a nearby site (8.26 mm, Panel C), at least three types of RGCs could be identified, including two cells with small somas and sparse dendritic fields (white arrowheads), two parasol cells (pink arrowheads), and

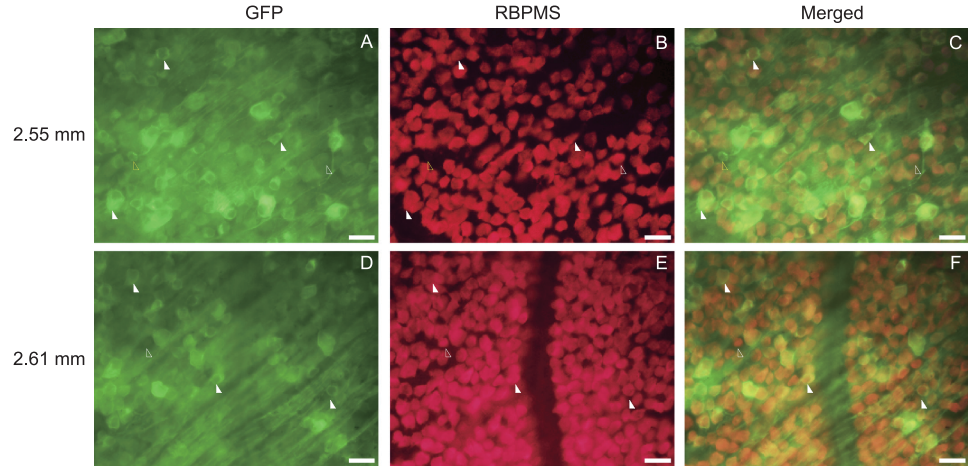

Figure 3 Quantitative analysis of double-labeled RGCs at central retinal locations beyond the fovea. Two central locations were sampled. Left column, GFP^+ RGCs. The center column reveals $RBPMS^+$ RGCs. The merged images in the right column were from images in the GFP and RBPMS columns. Eccentric distance to the fovea are shown to the left of the panels. Occasionally, some cells expressed GFP but not stained for RBPMS (yellow open arrowheads). Scale bar, 20 μm.

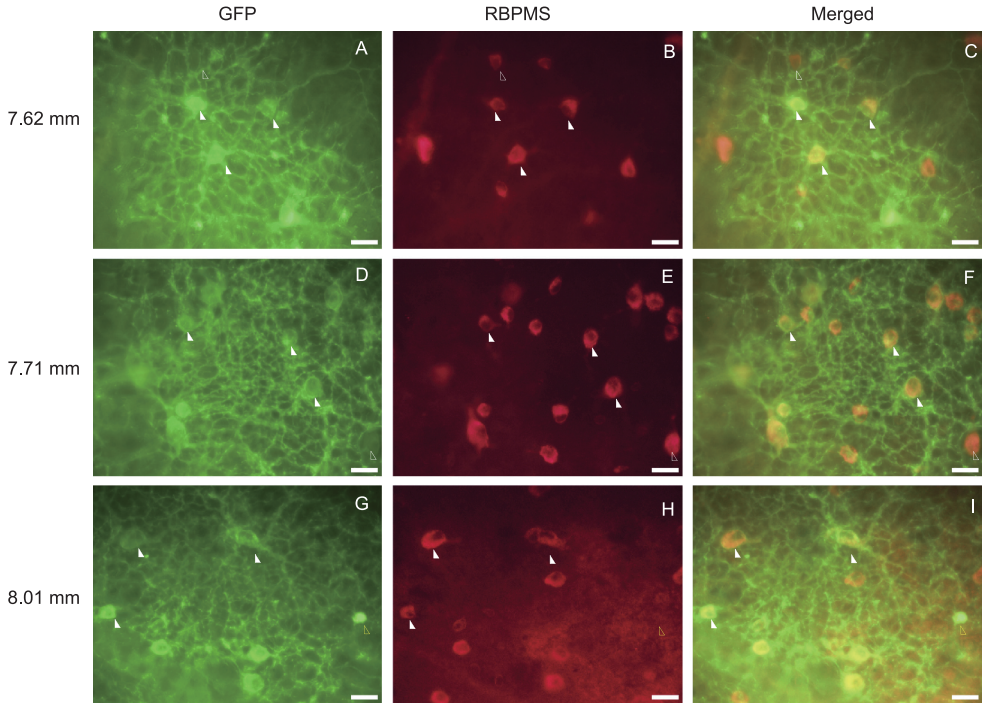

Figure 4 Quantitative analysis of double-labeled RGCs at peripheral retinal locations. Three peripheral locations were sampled. Left column, GFP^+ RGCs. The center column shows $RBPMS^+$ RGCs. The merged images are shown in the right column. Scale bar, 20 μm. Other conventions are as for Figure 3.

two midget cells (red arrowheads). Notice the strong color contrast between two cells indicated with pink arrowheads, suggesting that the depth difference between the two was approximately 80 μm. This may be an artifact due to tilting of the tissue. A cell with a dense dendritic field can be found at lower right corner of the graph (green arrow head). At 9.09 mm from the fovea, a cell (white arrow head) with large perikarya and dendritic field was positioned at the center of the filed (Panel D). The dendritic field overlapped with several neighboring midget cells. One of the cells with a large dendritic field was located at the center of the field, and the others with similar morphology were nearby. A cell with two primary dendritic processes and wavy dendritic branches was located in the upper right corner of the graph (purple arrowhead). However, these cells with large somas were encircled by another group of cells that had small somas but long and sparsely distributed dendritic processes (green arrowheads). At an eccentricity of 10.24 mm, three cells those had similar morphology were identified close together (red arrowheads, Panel E). Another cell with a soma of similar size had a dif-

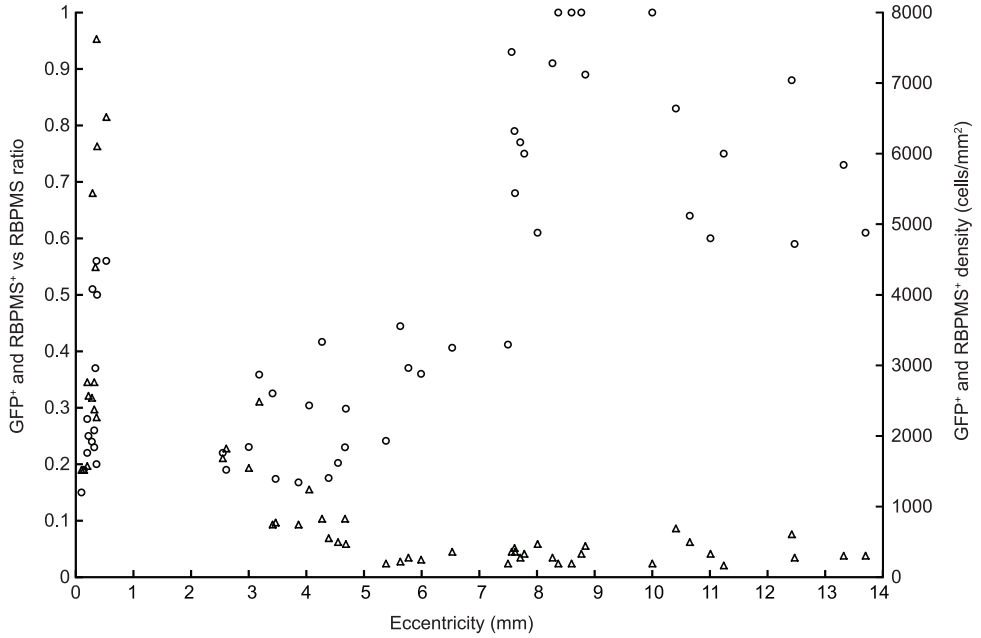

Figure 5 The ratio of encountering double-labeled versus RBPMS$^+$ RGCs and density variations of double-labeled RGCs at different eccentric retinal locations. The abscissa depicts retinal eccentricity and the ordinates depict the ratio of double-stained RGCs to RBPMS$^+$ RGCs (left) and the densities of double-labeled RGCs (right). The unfilled circles show the ratios and open triangles illustrate the density variations of double-labeled RGCs at different eccentricites.

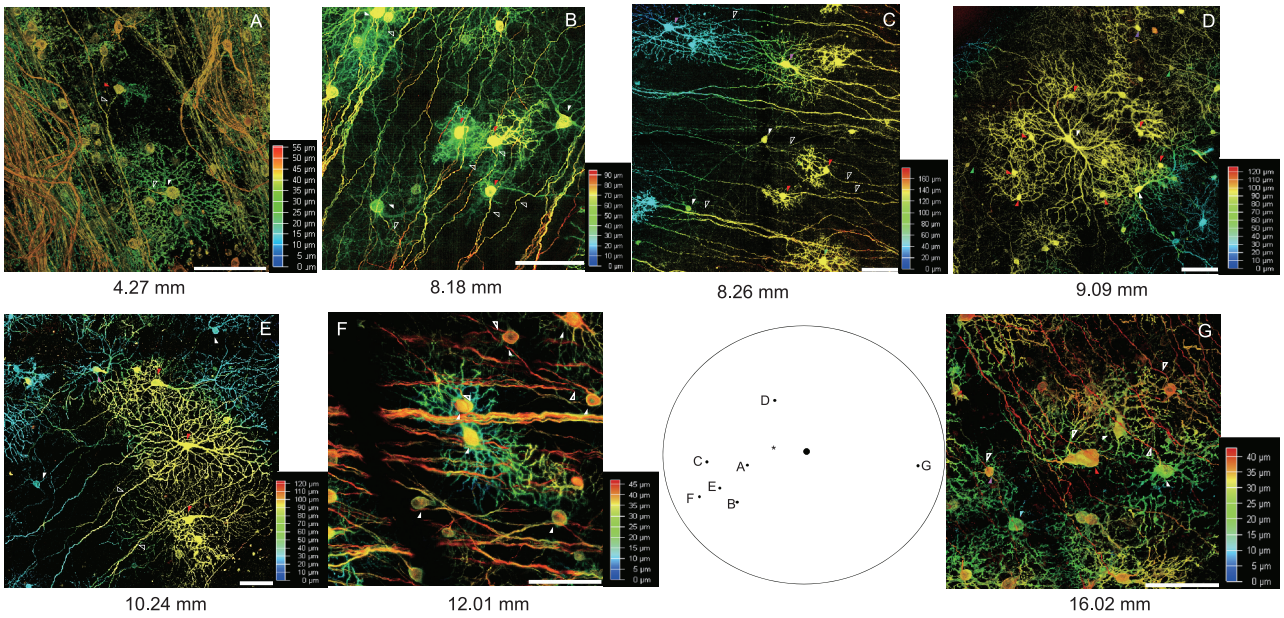

Figure 6 Multiple morphological types of GFP$^+$ RGCs at various eccentric retinal locations. A, One of the labeled cells showed midget cell morphology. Ecc, 4.27 mm. B, Three midget cells at center of the field were surrounded by three cells that shared similar dendritic morphologies. Ecc, 8.18 mm. C, At least three types of RGCs were illustrated in this micrograph. Ecc, 8.26 mm. D, A cell with large perikarya and dendritic field was located at the center of the filed. Ecc, 9.09 mm. E, Three cells shared similar morphology at nearby locations. Ecc, 10.24 mm. F, Most of the cells shared similar soma size and shape. Ecc, 12.01 mm. G, Different type of cells identified at remote peripheral retina. Ecc, 16.02 mm. All scale bars: 100 μm.

ferent dendritic branching pattern (pink arrowhead). Two cells were observed to share similar soma sizes but with completely different dendritic process densities (white arrowheads). At a more remote peripheral site (12.01 mm, Panel F), most of the cells share similar soma size and dendritic branching patterns. Two of them at the center field reveal typical midget cell morphology (white arrowhead). At the most remote peripheral sampling site (16.02 mm, Panel G), various types of RGCs were identified. The cell with the largest soma was at the center of the field (red arrowhead). Two more cells sharing similar soma morphology exhibited comparable dendritic processes. A cell with a smaller soma

and a different dendritic branching pattern was located below the cell with the large soma (cyan arrowhead). A cell with small soma was observed in the top right corner (green arrowhead). The cell with the smallest soma was observed to the left of the large cell (pink arrowhead). Interestingly, their somas were pseudocolored differently, suggesting these cell bodies were situated at different levels of the RGC layer.

DISCUSSION

The present study reveals that, by using GFP and RBPMS antibodies, the highest ratio of double-labeled RGCs at foveal sites reached 0.56. In the foveal region, most of the RGCs could be double-labeled within 200 μm of the inner edge of the fovea. However, few cells were GFP^+ at 400 μm from the edge. On the other hand, 0.78±0.16 (n=21 fileds) of RGCs at peripheral retinal sites could be double labeled (eccentricity >7 mm). Among the transgene expressing RGCs, midget and parasol cells were common. RGCs with diverse dendritic morphologies were frequently observed. Thus, as with wild-type ChR2, the present results suggest that this ChR2 transgene can be expressed in many morphologically distinct RGCs in this species of primate. Several retinal degenerative diseases cause incurable blinding, including age-related macular degeneration (Zaneveld et al., 2013; Chen and Zhang, 2015) and diabetic retinopathy (Kowluru and Mishra, 2015; Barber, 2015). This study offers valuable information for a clinically relevant gene therapy for these inner retinal degenerations.

The rate of double-stained RGCs at different eccentricities

The ring-like expression pattern of RGCs has been observed by several groups (Ivanova et al., 2010; Yin et al., 2011; Dalkara et al., 2009; Boyd et al., 2016). It has been reported that the number of transgene-expressing RGCs were concentrated at foveal region and that the density then gradually increased with eccentricity, but was very sparse in the remote peripheral retina (Yin et al., 2011). In agreement with previous reports that the double labeled RGCs showed relatively high expression in the foveal region. However, it should be noticed that, although there was only one layer of RGCs at the inner edge of the foveal region, multiple layers of RGCs were present at foveal locations. The present study suggests that the viral vector could only penetrate the superficial layer of RGCs away from the central fovea. Thus, although our data showed that, in the foveal region, the average rate of double-stained RGCs reached approximately 0.32, if multiple layers of foveal RGCs were taken into consideration, the rate could easily decrease substantially. Therefore, without using new approaches for viral penetration, the transgene could only be expressed in a small fraction of foveal RGCs. In the central retina, although our evidence reveals that the expression rate was approximately 0.20, few cells expressed GFP at eccentricities of 0.5 to 2. This may be due to a thick ILM (Wolter, 1964). On the other hand, in the peripheral retina, although we observed high rates of expression (from 0.80 and up to 1.00) in various retinas, the average expressing rates at all eccentricities was approximately 0.78.

Evaluate the transgene transmission with RBPMS antibody

One of the major issues of expressing trangenes in the retina is the non-specificity of the transmission of transgenes in the retina. Previous studies revealed that, in addition to RGCs, transgenes were expressed in many types of retinal neurons such as horizontal cells, amacrine cells and bipolar cells , as well as Müller cells (Bi et al., 2006; Ivanova and Pan, 2009; Ivanova et al., 2010). Their observations were confirmed by different investigators (Yin et al., 2011; Dalkara et al., 2009; Boyd et al., 2016). In particular, it was demonstrated that the area of transduction was restricted primarily to a "ring" of RGCs around the fovea (Ivanova et al., 2010; Yin et al., 2011; Dalkara et al., 2009; Boyd et al., 2016). However, to date, the exact number of ChR2-expressing RGCs remains to be determined. It has been reported that RBPMS could selectively label RGCs in monkey retina (Rodriguez et al., 2014). We used this antibody in the present study to quantify the transgene-expressing RGCs. As shown in Figures 1 through 4, RBPMS-immunoreactive cells were present from the foveal area to remote peripheral retinal locations. Occasionally, some cells expressed GFP but not RBPMS (Figure 3A–C, Figure 4G–I). Based on the morphological characteristics of these cells, they were either non-RGC neurons or non-neuronal Müller cells. Thus RBPMS could certainly help investigators to differentiate RGCs from other neurons or non-neuronal cells and serve as an effective RGC marker in future studies.

Morphological properties of the transgene expressed RGCs

Previous studies have revealed that many morphologically unique RGCs express wild-type ChR2 in mice and marmosets (Bi et al., 2006; Ivanova et al., 2010). The physiological response properties of the double mutant ChR2 L132C/T159C transgene were expressed in RGCs of marmosets (Ivanova et al., 2010). However, it remained to be determined if the mutant ChR2 L132C/T159C transgene can be expressed in RGCs of larger primate species such macaques. The present study shows that this transgene could be expressed in various types of retinal ganglion cells. As shown in Figure 6, midget and parasol cells were frequently observed. Several types of large field cells were also identified. Furthermore, we also observed several types of morphologically identical RGCs those formed their own networks. A detailed morphological classification of the transgene-expressing RGCs is underway in

our laboratory.

MATERIALS AND METHODS

DNA and viral vector constructs

The DNA and virus constructs of ChR2 mutations at the L132 and T159 sites (L132C/T159C) used in this study was described in detail in the previous article (Pan et al., 2014). Briefly, the DNA and virus constructs were created by gene synthesis (GenScript, USA) or site-directed mutagenesis (Agilent Technologies, USA). rAAV2 vectors carrying a fusion construct of ChR2 and GFP (ChR2-GFP) and driven by a CAG (a hybrid CMV early enhancer/chicken b-actin) promoter were modified from a previously reported construct (Bi et al., 2006). The virus vectors were packaged at Virovek (USA).

Animal preparation and intravitreal viral vector delivery

Nine young adult male cynomolgus macaques (*Macaca fascicularis*) were used in this study. Seven of them were 16 to 32 mon old and the other two were 39 and 50 mon old. The transgene expression was extremely weak for the two eldest and two young animals. Thus, data from these animals were excluded from further analysis. The other five animals showed reasonably good transgene expression, thus the rest of the article focuses on analysis of data collected from these animals. All animal experiments and procedures were approved by the Institutional Animal Care and Use Committee of Peking University and were performed in accordance with the ARVO Statement for the Use of Animals in Ophthalmic and Vision Research. The animals were anesthetized by intramuscular injection of ketamine (1 mg/100 g body weight). The rAAV2 viral vector (50 μL) carrying the L132C/T159C transgenes at a concentration of 1.0×10^{13} vg mL^{-1} was injected into the vitreous chamber with a 100 μL Hamilton syringe using a 33-gauge sharp-point needle (model #65460-20, Hamilton company, USA). The intravitreal injection site was chosen on the temporal side of the eyeball, 2 mm posterior to the limbus. The injections were administered slowly over approximately 10 min.

Two to three months after viral injection, animals were intramuscularly injected with 20 mg kg^{-1} ketamine and 5 mg kg^{-1} xylazine, then the eyes were enucleated. Animals were euthanized by intra-cardial injection of pentobarbital (100 mg kg^{-1} body weight).

Whole-mount retina preparation

Enucleated eyes were fixed in 4% paraformaldehyde (Cat. No. 15710, Electron Microscopy Sciences, USA) in phosphate buffer (PB) at room temperature for 60 min. After the cornea, lens, and vitreous body were removed, the whole-mount retina was dissected from the RPE. Several radial relieving cuts were made through the peripheral retina. Whole-mount retinas were then washed four times with 0.1 mol L^{-1} PBS (1×; 85 mmol L^{-1} Na_2HPO_4, 15 mmol L^{-1} NaH_2PO_4, 150 mmol L^{-1} NaCl, pH 7.4) for 10 min per wash on a shaker (unless otherwise stated, all steps in the following protocol were performed on a shaker). The retinas were mounted on glass slides with the ganglion cell layer up, air-dried, and coverslipped using antifade mounting medium (Cat. No. 17985-11, Electron Microscopy Sciences).

Immunohistochemistry

The retinas were washed six times (6× 10 min with 0.1 mol L^{-1} PBS) on a shaker at room temperature, blocked for 48 h at 4°C, and incubated in a solution containing anti-GFP and anti-RBPMS antibodies for seven days at 4°C. Details of the staining techniques have been described elsewhere (Wang et al., 2016). Briefly, the retinas were placed in 10% blocking medium (008120, Life Technology Inc., USA) in 0.3% Triton-X-100 and phosphate-buffered saline mixture (Vector Laboratories Inc., USA) for 48 h before incubating with primary antibodies: anti-GFP polyclonal antibody (1:1000, AB183734, Abcam Corp, UK) and anti-RBPMS antibody (1:1000, ProSci, USA) for seven days at 4°C. After rinsing six times as described above to remove excess primary antibody, the retinas were then incubated with secondary antibodies including DI-1488-conjugated IgG (1:500, Vector Labortories Inc., USA) and Alex Fluor 568 (A11075, 1:1000, Life Technology, USA) overnight at 4°C. After washing an additional six times as described above, the free floating retinas were mounted on slides, immersed in anti-fade mounting medium (#17985-11, Electron Microscopy Sciences) and covered with a cover slip (#63772-01, Electron Microscopy Science).

Qualitative and quantitative analysis of GFP expressing RGCs

The distribution of dendritic processes and the ramification patterns of RGCs expressing GFP were quantitatively analyzed by using either a high resolution laser-scaning confocal microscope (Leica TCS-SP8, Germany) or a conventional fluorescent microscope (Olympus BX51, Olympus, Japan). Under the fluorescent microscope, the dendritic morphology of a given GFP-expressing RGC was measured. For confocal microscope, with use of a 40× or 63× oil immersion objective (Leica), a series of optical sections was collected from an area of 290×290 μm or 155×155 μm respectively at Z-axis intervals of 0.3 μm. Each section was averaged two times. Because the dendritic field size of GFP expressing cells was larger than the maximum scanning area, a sequential scanning that covered the whole dendritic field was performed.

For most cells the range of sampling in the *Z*-axis was maintained at 100 μm, which extended from the GCL through the IPL and ended in the INL.

Compliance and ethics *The author(s) declare that they have no conflict of interest.*

Acknowledgements *This work was supported by National Science Foundation of China (31571091 to Mingliang Pu), National Basic Research Program of China (2015CB351806 to Mingliang Pu), National Institutes of Health Grant (NIH) (EY17130 to Zhuo-Hua Pan), Dryer Foundation, the Ligon Research Center of Vision, and Research to Prevent Blindness to Department of Ophthalmology at Wayne State University.*

Barber, A.J. (2015). Diabetic retinopathy: recent advances towards understanding neurodegeneration and vision loss. Sci China Life Sci 58, 541–549.

Berndt, A., Schoenenberger, P., Mattis, J., Tye, K.M., Deisseroth, K., Hegemann, P., and Oertner, T.G. (2011). High-efficiency channelrhodopsins for fast neuronal stimulation at low light levels. Proc Natl Acad Sci USA 108, 7595–7600.

Bi, A., Cui, J., Ma, Y.P., Olshevskaya, E., Pu, M., Dizhoor, A.M., and Pan, Z.H. (2006). Ectopic expression of a microbial-type rhodopsin restores visual responses in mice with photoreceptor degeneration. Neuron 50, 23–33.

Boyd, R.F., Boye, S.L., Conlon, T.J., Erger, K.E., Sledge, D.G., Langohr, I.M., Hauswirth, W.W., Komáromy, A.M., Boye, S.E., Petersen-Jones, S.M., and Bartoe, J.T. (2016). Reduced retinal transduction and enhanced transgene-directed immunogenicity with intravitreal delivery of rAAV following posterior vitrectomy in dogs. Gene Ther 23, 548–556.

Buie, L.K.K., Rasmussen, C.A., Porterfield, E.C., Ramgolam, V.S., Choi, V.W., Markovic-Plese, S., Samulski, R.J., Kaufman, P.L., and Borrás, T. (2010). Self-complementary AAV virus (scAAV) safe and long-term gene transfer in the trabecular meshwork of living rats and monkeys. Invest Ophthalmol Vis Sci 51, 236.

Chen, Z.G., and Zhang, Y.A. (2015). Cell therapy for macular degeneration—first phase I/II pluripotent stem cell-based clinical trial shows promise. Sci China Life Sci 58, 119–120.

Dalkara, D., Kolstad, K.D., Caporale, N., Visel, M., Klimczak, R.R., Schaffer, D.V., and Flannery, J.G. (2009). Inner limiting membrane barriers to AAV-mediated retinal transduction from the vitreous. Mol Ther 17, 2096–2102.

Ivanova, E., and Pan, Z.H. (2009). Evaluation of the adeno-associated virus mediated long-term expression of channelrhodopsin-2 in the mouse retina. Mol Vis 15, 1680–1689.

Ivanova, E., Hwang, G.S., Pan, Z.H., and Troilo, D. (2010). Evaluation of AAV-mediated expression of Chop2-GFP in the marmoset retina. Invest Ophthalmol Vis Sci 51, 5288.

Jacobson, S.G., Boye, S.L., Aleman, T.S., Conlon, T.J., Zeiss, C.J., Roman, A.J., Cideciyan, A.V., Schwartz, S.B., Komaromy, A.M., Doobrajh, M., Cheung, A.Y., Sumaroka, A., Pearce-Kelling, S.E., Aguirre, G.D., Kaushal, S., Maguire, A.M., Flotte, T.R., and Hauswirth, W.W. (2006). Safety in nonhuman primates of ocular AAV2-*RPE65* , a candidate treatment for blindness in Leber congenital amaurosis. Hum Gene Ther 17, 845–858.

Kleinlogel, S., Feldbauer, K., Dempski, R.E., Fotis, H., Wood, P.G., Bamann, C., and Bamberg, E. (2011). Ultra light-sensitive and fast neuronal activation with the Ca^{2+}-permeable channelrhodopsin CatCh. Nat Neurosci 14, 513–518.

Kowluru, R.A., and Mishra, M. (2015). Contribution of epigenetics in diabetic retinopathy. Sci China Life Sci 58, 556–563.

Kwong, J.M.K., Caprioli, J., and Piri, N. (2010). RNA binding protein with multiple splicing: a new marker for retinal ganglion cells. Invest Ophthalmol Vis Sci 51, 1052.

Lai, C.M., Shen, W.Y., Brankov, M., Lai, Y.K.Y., Barnett, N.L., Lee, S.Y., Yeo, I.Y.S., Mathur, R., Ho, J.E.S., Pineda, P., Barathi, A., Ang, C.L., Constable, I.J., and Rakoczy, E.P. (2005). Long-term evaluation of AAV-mediated sFlt-1 gene therapy for ocular neovascularization in mice and monkeys. Mol Ther 12, 659–668.

Lin, J.Y., Lin, M.Z., Steinbach, P., and Tsien, R.Y. (2009). Characterization of engineered channelrhodopsin variants with improved properties and kinetics. Biophys J 96, 1803–1814.

Liu, R., Wang, Y., Pu, M., and Gao, J. (2016). Effect of alpha lipoic acid on retinal ganglion cell survival in an optic nerve crush model. Mol Vision 22, 1122–1136.

Maclachlan, T.K., Lukason, M., Collins, M., Munger, R., Isenberger, E., Rogers, C., Malatos, S., Dufresne, E., Morris, J., Calcedo, R., Veres, G., Scaria, A., Andrews, L., and Wadsworth, S. (2011). Preclinical safety evaluation of AAV2-sFLT01—A gene therapy for age-related macular degeneration. Mol Ther 19, 326–334.

Mattis, J., Tye, K.M., Ferenczi, E.A., Ramakrishnan, C., O'Shea, D.J., Prakash, R., Gunaydin, L.A., Hyun, M., Fenno, L.E., Gradinaru, V., Yizhar, O., and Deisseroth, K. (2011). Principles for applying optogenetic tools derived from direct comparative analysis of microbial opsins. Nat Meth 9, 159–172.

Nagel, G., Ollig, D., Fuhrmann, M., Kateriya, S., Musti, A.M., Bamberg, E., and Hegemann, P. (2002). Channelrhodopsin-1: a light-gated proton channel in green algae. Science 296, 2395–2398.

Nagel, G., Szellas, T., Huhn, W., Kateriya, S., Adeishvili, N., Berthold, P., Ollig, D., Hegemann, P., and Bamberg, E. (2003). Channelrhodopsin-2, a directly light-gated cation-selective membrane channel. Proc Natl Acad Sci USA 100, 13940–13945.

Nagel, G., Brauner, M., Liewald, J.F., Adeishvili, N., Bamberg, E., and Gottschalk, A. (2005). Light activation of channelrhodopsin-2 in excitable cells of *Caenorhabditis elegans* triggers rapid behavioral responses. Curr Biol 15, 2279–2284.

Pan, Z.H., Ganjawala, T.H., Lu, Q., Ivanova, E., and Zhang, Z. (2014). ChR2 mutants at L132 and T159 with improved operational light sensitivity for vision restoration. PLoS ONE 9, e98924.

Piri, N., Kwong, J.M.K., Song, M., and Caprioli, J. (2006). Expression of hermes gene is restricted to the ganglion cells in the retina. Neurosci Lett 405, 40–45.

Rodriguez, A.R., de Sevilla Müller, L.P., and Brecha, N.C. (2014). The RNA binding protein RBPMS is a selective marker of ganglion cells in the mammalian retina. J Comp Neurol 522, 1411–1443.

Wang, H., Sugiyama, Y., Hikima, T., Sugano, E., Tomita, H., Takahashi, T., Ishizuka, T., and Yawo, H. (2009). Molecular determinants differentiating photocurrent properties of two channelrhodopsins from chlamydomonas. J Biol Chem 284, 5685–5696.

Wang, Y., Wang, W., Liu, J., Huang, X., Liu, R., Xia, H., Brecha, N.C., Pu, M., and Gao, J. (2016). Protective effect of ALA in crushed optic nerve cat retinal ganglion cells using a new marker RBPMS. PLoS ONE 11, e0160309.

Weber, M., Rabinowitz, J., Provost, N., Conrath, H., Folliot, S., Briot, D., Chérel, Y., Chenuaud, P., Samulski, J., Moullier, P., and Rolling, F. (2003). Recombinant adeno-associated virus serotype 4 mediates unique and exclusive long-term transduction of retinal pigmented epithelium in rat, dog, and nonhuman primate after subretinal delivery. Mol Ther 7, 774–781.

Wolter, J.R. (1964). Pores in the internal limiting membrane of the human retina. Acta Ophthalmol 42, 971–974.

Ye, G., Budzynski, E., Sonnentag, P., Nork, T.M., Miller, P.E., Sharma, A.K., Ver Hoeve, J.N., Smith, L.M., Arndt, T., Calcedo, R., Gaskin, C., Robinson, P.M., Knop, D.R., Hauswirth, W.W., and Chulay, J.D. (2016). Safety and biodistribution evaluation in *Cynomolgus macaques* of rAAV2tYF-PR1.7-hCNGB3, a recombinant AAV vector for treatment of achromatopsia. Hum Gene Ther Clin Dev 27, 37–48.

Yin, L., Greenberg, K., Hunter, J.J., Dalkara, D., Kolstad, K.D., Masella, B.D., Wolfe, R., Visel, M., Stone, D., Libby, R.T., DiLoreto Jr, D., Schaffer, D., Flannery, J., Williams, D.R., and Merigan, W.H. (2011).

Intravitreal injection of AAV2 transduces macaque inner retina. Invest Ophthalmol Vis Sci 52, 2775.

Yizhar, O., Fenno, L.E., Prigge, M., Schneider, F., Davidson, T.J., O'Shea, D.J., Sohal, V.S., Goshen, I., Finkelstein, J., Paz, J.T., Stehfest, K., Fudim, R., Ramakrishnan, C., Huguenard, J.R., Hegemann, P., and Deisseroth, K. (2011). Neocortical excitation/inhibition balance in information processing and social dysfunction. Nature 477, 171–178.

Zaneveld, J., Wang, F., Wang, X., and Chen, R. (2013). Dawn of ocular gene therapy: implications for molecular diagnosis in retinal disease. Sci China Life Sci 56, 125–133.

Zhang, F., Prigge, M., Beyrière, F., Tsunoda, S.P., Mattis, J., Yizhar, O., Hegemann, P., and Deisseroth, K. (2008). Red-shifted optogenetic excitation: a tool for fast neural control derived from *Volvox carteri*. Nat Neurosci 11, 631–633.